SAND2019-13787C

Title: Temperature Dependent X-ray Fluorescent Response from Thermographic Phosphors under X-ray Excitation

Authors: Eric R. Westphal, Alex D. Brown, Enrico C. Quintana, Alan L. Kastengren, Steven F. Son, Terrence R. Meyer, and Kathryn N. G. Hoffmeister

Colloquium: Diagnostics

Word equivalent lengths:

Main text: 2795 words

Equations: 0 words

Nomenclature: 0 words

References: 612 words

Tables: 0 words

Figures: 1608 words

Total length of paper: 5015 words

Supplemental material available

Abstract:

Phosphor thermometry has been successfully applied within several challenging environments, including some combusting flows. In this approach, the visible emission from thermographic phosphors excited by an ultraviolet laser can be measured and the spectral or temporal response correlated to temperature. However, issues exist within optically obscured environments, in which the signal can be scattered by particulates or reabsorbed and reemitted outside of the intended measurement volume. In addition, emission from the flame may interfere with the phosphor emission. A temperature dependent x-ray excitation/emission could alleviate these issues as x-rays could penetrate obscurants and flames do not emit in these wavelengths. In addition, this type of emission could potentially allow for thermometry within solid propellants or energetic materials simultaneously with x-ray imaging of the structural evolution. In this study, several thermographic phosphors were excited via x-ray radiation, and their x-ray emission characteristics were measured at varying temperatures. Several of the phosphors showed varying levels of temperature dependence, with the strongest sensitivity occurring for YAG:Dy and $ZnGa_2O_4$:Mn. This opens a new path for non-intrusive temperature measurements in optically opaque multiphase or solid phase combustion environments.

Keywords: X-rays, thermographic phosphors, x-ray fluorescence

1. Introduction

Conventional phosphor thermometry is a temperature sensing technique involving the excitation of thermographic phosphor particles via a light source in the ultraviolet (UV) or near UV range [1–5]. When excited, the phosphors undergo electronic energy level transitions to a higher energy state, followed by relaxation back to the ground state accompanied by the emission of photons that are red-shifted from the excitation source. Depending on the phosphor temperature, the emission spectrum can broaden or shift in wavelength or intensity. Both the phosphor's fluorescence lifetime and spectral profile are temperature dependent, and either can be used for thermometry after proper calibration [3,6].

All phosphors vary in composition, though they generally follow the same structure in which a ceramic host matrix is doped with either a transition metal or rare-earth element. The luminescence from the phosphors typically originates from the dopant (also called the activator), while the host ceramic remains relatively transparent to the incident or induced radiation [3]. However, the key to the temperature dependence of the induced emission is the interaction during relaxation between the ceramic matrix and within the crystal structure, which affect the relative radiative and non-radiative energy transfer processes during relaxation to the ground state [2]. Increases in internal energy of the phosphor particles at elevated temperature cause the non-radiative processes to vary with temperature, leading to temperature dependent emission.

Conventional phosphor thermometry has been employed to measure temperature within combustion and heated environments, such as diesel engines [7–9], gas turbines [10–13], and gaseous flows [14–17]. However, traditional excitation and emission schemes will fail in optically thick gaseous flow conditions or within reacting opaque solids, and an alternative approach is needed for non-intrusive measurements.

X-rays are sufficiently energetic to pass through many solid materials and optical absorbers that inhibit UV or near-UV excitation. UV photon excitation causes energy level transitions from the valence electrons of the phosphor particles. The energy gap between these transitions correspond to the frequency of the red-shifted near-UV or visible emission produced by the phosphors. However, incident x-ray radiation has sufficient energy to penetrate further into the atoms composing the phosphors and to interact with K-shell electrons. This can

cause x-ray fluorescence (XRF), which gives rise to x-ray emission spectroscopy (XES), in which K-shell electrons are ejected from the atoms due to the incident x-rays [18,19]. An outer-shell electron then fills this vacancy, producing an x-ray photon during the transition. The energies of x-rays produced in this manner are characteristic to the element of the atom being excited.

As x-ray excitation penetrates deep into the core of atoms, the characteristic x-ray emission produced is typically considered to be independent of temperature. This approximation can break down in crystalline structures containing transition metals and rare-earth elements, in which core holes left by the x-ray excitation couple strongly with valence electrons [20]. Since the core hole is coupled with valence electrons, final energy states available to electrons filling the hole are dependent on the location of the valence electron shell positions, leading to temperature dependence as seen in Figure 1. In these complex systems, spin pairing, material structure, insulator-metal transitions, and electronic screening lead to temperature- and pressure-dependent transitions that affect the structure of the characteristic x-ray lines [21–25].

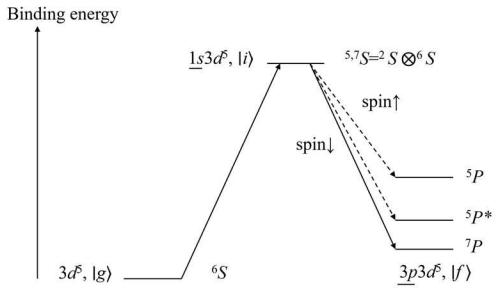

Figure 1. K_β process (3p→1s) in the case of a $3d^5$ ion reproduced from [24]. Reprinted figure from Ruefe and Shukla, Review of Modern Physics, Volume 82, pg. 864, 2010. Copyright 2010 by the American Physical Society.

In the case of d-electron materials (those containing elements with unfilled d-shells such as Y, Ce, Mn, etc.), particularly oxides, the average electron distance is much greater than the Bohr radius, creating strong electron-electron repulsion [25]. D shells have internal degrees of freedom, which when coupled into a lattice structure, can lead to strong movement coupling effects between electrons in materials, known as electron correlation.

Where electron correlation is high, electronic transitions, including those involved in x-ray spectroscopy, have high susceptibility to temperature, pressure, magnetic fields, and doping effects. In these d-electron materials, the K_β (3p→1s) and K_α (2p→1s) transitions are shown to be sensitive to transition-metal spin state [21–25]. See Ref [24] for a detailed description of the multiplet spin structure. F-electron systems, materials with partially filled 4f and 5f shells such as Dy, Eu, etc., have also shown strong electron correlation [24,25].

If phosphor XRF is thermographic, in a similar manner to their visible emission, temperature measurements could be made of a sample contained within an opaque boundary – e.g. oven walls, sooty flames, or solid rocket fuel. The limiting factor would become collection of the x-rays produced by the phosphors, which should have sufficient energy to pass through the boundary. In addition, x-ray excitation would allow for simultaneous temperature measurement and x-ray imaging of a sample structure that may be undergoing dynamic deformation. However, while the pressure effects and material/chemical transitions have been well characterized in UV and visible emissions [26], these effects would have to be studied in detail in the x-ray regime. The objective of this work is to determine the temperature sensitivity of a wide range of thermographic phosphors during x-ray excitation/emission at atmospheric pressures. To the authors' knowledge, the XRF emissions from phosphors have never been characterized for temperature dependence.

2. Experimental Methods

2.1 Phosphor Selection and Sample Preparation

Phosphors selected for testing were chosen based on the desired applications and x-ray excited optical emission (XEOL). Of the phosphors used in this study, YAG:Dy (PTL QMK66), $BaMgAl_{10}O_{17}$:Eu (also known as BAM, PTL KEMK63), La_2SO_4:Eu (PTL SKL63), $Mg_3F_2GeO_4$:Mn (PTL EQD25), $ZnGa_2O_4$:Mn (PTL GPK25), and ZnO (Just Pigments, ZN001-1), were selected based on their usefulness to combustion applications [14,27–29]. In addition, the phosphors Gd_2O_2S:Tb (PTL UKL65) and Y_2SiO_5:Ce (PTL QBK58) were selected for their usefulness as x-ray scintillators, materials used in x-ray detectors that change x-rays to visible light [30–32]. The results for La_2SO_4:Eu, $Mg_3F_2GeO_4$:Mn, and Y_2SiO_5:Ce are included in the supplemental materials.

Phosphors were tested independently. Each sample was prepared by mixing a phosphor powder with ethanol. A brush was then used to coat the mixture onto an aluminum substrate and allowed to dry. Aluminum was selected due to the low energies of its characteristic x-ray emission lines (<2 keV). This avoids interference between potentially thermographic emission lines originating from the transition metals and rare-earth elements (typically >5 keV in the materials tested) in the phosphors and the substrate.

2.2 Excitation/Detection Setup

Once prepared, phosphor samples were then placed on a hot plate alongside a blank aluminum substrate, as shown in Figure 2. This blank substrate was used for collecting background energy spectra subtracted during later data post processing. A thermocouple was placed on the surface of the hot plate between the coated and blank aluminum substrates to monitor the sample temperatures as each was heated and cooled. This setup was placed in the path of the x-ray beam in beamline 7-BM-B at the Advanced Photon Source at Argonne National Laboratory. This beamline was set to monochromatic beam mode during phosphor excitation, producing x-rays at 67.6 keV with a 1% bandpass. Monochromatic beam mode was chosen to reduce the effects of the beam energy profile on the measurements. A Vortex silicon drift x-ray detector (Hitachi) was used to capture the energy spectra of the x-ray fluorescence produced by each phosphor and substrate. The incident x-rays were attenuated with various combinations of Si, Cu, and Ge filters to optimize the intensity of the x-ray signal detected for each phosphor and to test whether incident flux was changing the shape of the detected XRF emission. During testing, background and phosphor signal spectra were captured at each temperature and for each phosphor. A total of 10 background spectra and 50 phosphor signal spectra were obtained at each temperature for signal averaging. All spectra presented in the results of this study were averaged (unless specified otherwise) and background subtracted. The hot plate was placed on a computer-controlled translation stage which allowed the signal to be captured at the same locations.

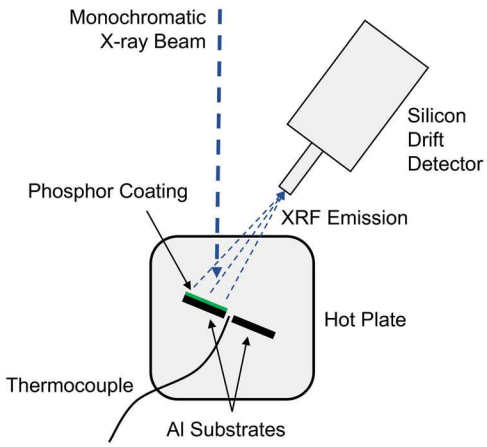

Figure 2. Set-up for x-ray excitation and emission detection at the Advanced Photon Source.

3. Results and Discussion

3.1 YAG:Dy

YAG:Dy was tested at temperatures ranging from room temperature up to 333 °C, and the averaged x-ray spectra captured in this range are seen in Figure 3. The peaks seen in Figure 3a are labeled with their corresponding emission line transitions. Similar labels are used throughout this paper for each phosphor tested and their resulting emission lines. Note that lines labeled 'K_α' are made up of the $K_{\alpha1}$ and $K_{\alpha2}$ peaks of the corresponding element. Emission lines such as these that cannot be resolved individually by the x-ray detector and are grouped together in this way throughout this paper. The spectra shown in Figure 3a are normalized to the intensity of the dysprosium (Dy) L_α peak at each temperature centered at about 6.5 keV. The Y K_α line can clearly be seen to shift in intensity with temperature, whereas the yttrium (Y) $K_{\beta1}$ remains relatively constant over the temperature range. These results suggest that an intensity ratio calculated using the Y K_α and Dy L_α peaks and potentially could be used for phosphor thermometry. Also shown is the non-normalized data for the Y K_α peak (see Figure 3b). While temperature dependence is not seen in the Y $K_{\beta1}$ peak at the temperatures measured in this study, the significant broadening and line shape asymmetry suggests that its linewidth is temperature dependent [24].

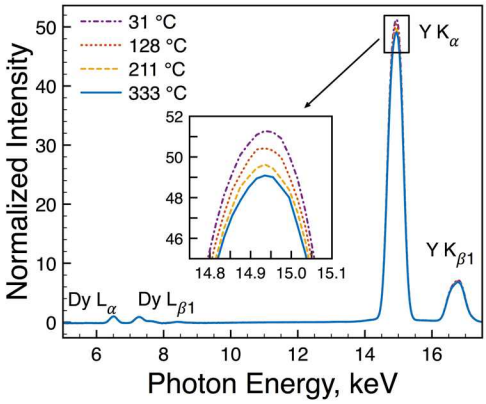

a)

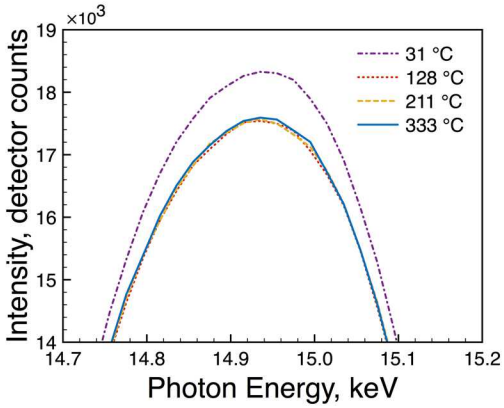

b)

Figure 3. X-ray energy spectra of YAG:Dy at various temperatures. a) The overall spectra (normalized) and b) the non-normalized spectra of the Y K_α peak.

3.2 $BaMgAl_{10}O_{17}$:Eu

The overall spectra of the x-ray emission from BAM is shown in Figure 4a. The spectra are normalized to the barium (Ba) $K_{\beta1}$ peak. No temperature sensitivity can be seen in the Ba K_α line of the normalized data, however, the Ba L_α and Ba $L_{\beta1}$ lines do appear to be thermographic, as seen in the subplot in Figure 4a. This sensitivity is likely due to interactions with the unfilled f shell of the europium (Eu) atoms, whose K lines were beyond our detection limits. The temperature sensitivity of these lines is relatively weak, however, as indicated by Figure 4b, showing all the spectra captured at each temperature. A general trend can be seen in the spectra showing a direct

relationship between line intensity and temperature. However, a large amount of overlap can be seen between the spectra at each temperature, indicating large inaccuracies would persist in any temperature measurements made using these XRF lines of BAM at these temperatures. Note that the spectra in Figure 4c are not normalized.

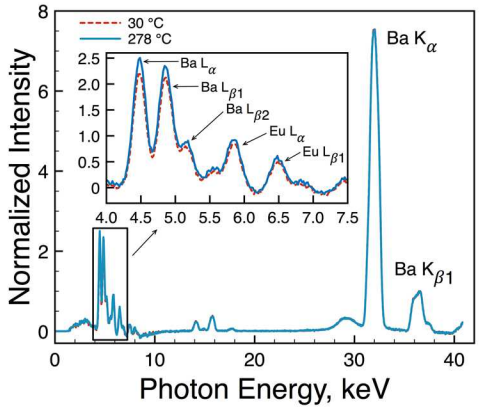

a)

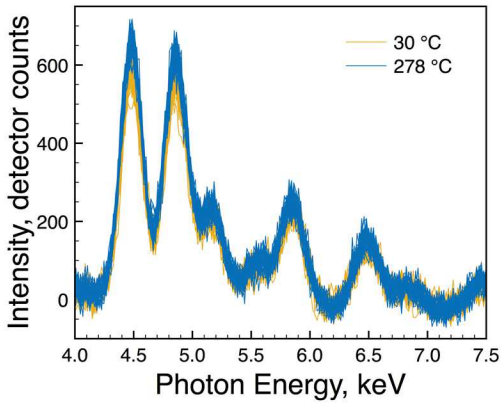

b)

Figure 4. The x-ray energy spectra of BAM at various temperatures. a) The normalized overall spectra and the normalized spectra showing the emission lines at lower energies in more detail (subplot), and b) all the spectra captured at each temperature (note that this last plot is not normalized).

3.3 Gd_2O_2S:Tb

Gd_2O_2S:Tb is both a low-temperature thermographic phosphor when excited with UV radiation and known to produce optical emission under x-ray excitation. The primary use of Gd_2O_2S:Tb is as an x-ray scintillator to convert

x-ray photons to visible light for x-ray imaging due its strong x-ray absorption at the gadolinium (Gd) K-edge [33]. At 50 keV, this K-edge was outside of the range of the x-ray detector used in this study, limiting our ability to fully investigate the most likely source of temperature dependence for this phosphor. Signal from the Gd L-edge emission lines normalized to the Gd $L_{\gamma 1}$ peak can be seen in the results for this phosphor in Figure 5. No significant temperature dependence can be seen at temperatures corresponding to the thermographic range of Gd_2O_2S:Tb when excited with UV light [27,28]. Testing of this phosphor with a higher-keV range detector and larger temperature range is necessary to rule out its temperature sensitivity.

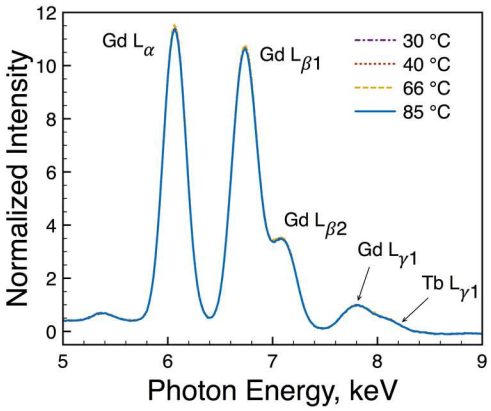

Figure 5. The normalized x-ray energy spectra of Gd_2O_2S:Tb at various temperatures.

3.4 $ZnGa_2O_4$:Mn

Results for $ZnGa_2O_4$:Mn normalized over the Ga $K_{\beta 1}$ emission line are seen in Figure 6. This phosphor differs from all others presented thus far in that it is doped with a transition metal rather than a rare-earth element, though the partially-filled d shell of manganese (Mn) suggests that the physics leading temperature-dependence should be similar. Mn lines were not sufficiently separated from other emissions to be usable and thus are not shown in the figure. Both the gallium (Ga) and zinc (Zn) K_α lines exhibit some degree of temperature sensitivity with this normalization.

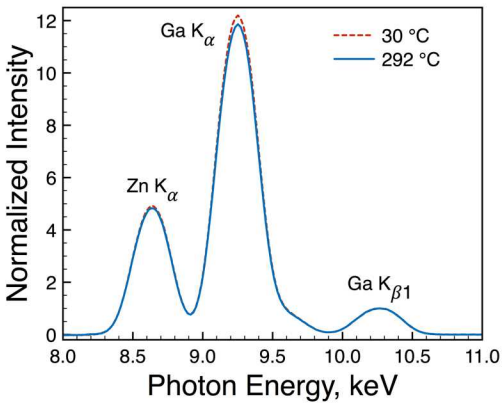

Figure 6. The normalized x-ray energy spectra of $ZnGa_2O_4$:Mn at various temperatures.

3.5 ZnO

Though undoped, pure ZnO is known to produce a thermographic optical emission [29]. However, Zn does not have the properties (unfilled d or f shells) that would suggest thermographic response in the x-ray spectrum. The normalized energy spectra obtained for this phosphor are shown in Figure 7, along with a plot showing non-normalized spectra. No temperature dependence is seen in the data when normalized, though significant changes in intensity are seen in the non-normalized data (Figure 7b). Note that two average spectra at 30 °C are shown in the non-normalized data. These two spectra differ in the time they were captured. One was collected before any heating of the sample had occurred (BH) and the other was captured after the sample had been heated to its maximum temperature of 282 °C and then allowed to cool back down to 30 °C (AC). The significant hysteresis in the data suggests that ZnO may have undergone a chemical transition similar to that seen in $LaCoO_3$ in Ref. [22].

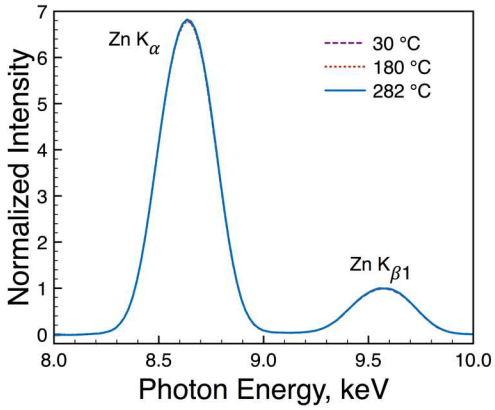

a)

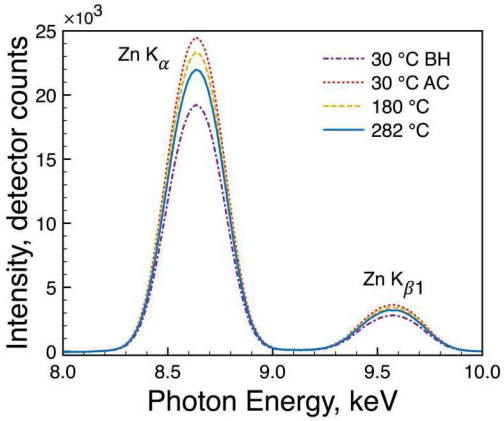

b)

Figure 7. The x-ray energy spectra of ZnO at various temperatures. a) The normalized data and b) non-normalized data showing the spectra at each temperature including two sets of data obtained at 30 °C, one before the sample was subjected to any heating (BH) and another after the sample was heated to the maximum temperature of 282 °C and allowed to cool back down to 30 °C (AC).

3.6 Discussion of Results

From these initial experiments, it appears that the best candidates for temperature sensing using x-ray excitation/emission are YAG:Dy and $ZnGa_2O_4$:Mn for the configuration considered; both exhibit clear temperature sensitivity in their XRF responses. Alternatively, it may be possible to utilize multiple phosphors with and without temperature sensitivity in combination to achieve the same result. Other materials, particularly those with dopants whose K-level emission lines were beyond our detection limits, may also be viable options. The K-level emission lines of dopants would be particularly useful for scenarios with significant optical access challenges, as the harder x-ray emissions will better penetrate the optical obstruction.

The results described here are consistent with the hypothesis that complex spin-state multiplet structures are responsible for temperature-dependence in the x-ray region [24]. Supporting this hypothesis is the lack of temperature response in ZnO, as it is the only material tested that does not have a matrix containing elements

with partially filled d/f shells. This suggests that while many of the known optically thermographic materials meet the requirements for x-ray temperature dependence (complex crystal matrices with elements containing partially filled d/f shells, particularly those in oxide form or dopants), researchers should not limit themselves to these materials. Another key consideration is that due to the strong pressure-dependence of this mechanism, future research in the x-ray spectrum must take pressure into account when determining the viability of these materials.

Temperature ranges tested in this study were selected in part based on the ranges of sensitivity of the visible response from these phosphors. However, based on the results for Gd_2O_2S:Tb, this may not be a good indication for the sensitivity of the x-ray response, as the x-ray emission of this phosphor showed no temperature sensitivity over this range, though there may be temperature-sensitive emissions at higher x-ray energies beyond the range of the detector used in this study.

All measurements in this paper were collected with the monochromatic beam at APS. An important consideration for measurements using lab-scale or medical x-ray excitation will be the spectrum of the incident photons. A broadband spectrum that includes energies of the XRF emission lines studied will need to be convolved in order to make the technique independent of excitation source.

4. Conclusion

The x-ray energy spectra of several thermographic phosphors were measured at various temperatures during x-ray excitation. The characteristic x-ray emission lines of several of these phosphors showed varying degrees of temperature sensitivity. Based on these initial results, the two primary candidates for future characteristic x-ray based temperature sensing measurements are YAG:Dy and $ZnGa_2O_4$:Mn. Other phosphors may show temperature sensitive emission intensity that was uniform among the measured transitions, which prevented an intensity independent temperature measurement using line ratios. However, it may be possible to utilize combinations of phosphors with and without temperature sensitivity to broaden the materials that could be utilized for this purpose. Another option would be to utilize off-peak locations within the spectra of phosphors with a thermographic x-ray emission line to create a temperature sensitive intensity ratio. The results were consistent

with changes in the x-ray emission spectrum being dependent on multiplet structure, as described in previous studies [21–25]. Extended temperature ranges should be investigated in the future for all the phosphors tested here to determine if their sensitivity lies in or extends into a region beyond those in this study.

Acknowledgements

The authors would like to thank the Office of Naval Research as this research is funded, in part, through project Award No. N00014-16-1-2557, and by the Air Force Office of Scientific Research through Award No. FA9550-15-1-0102 to Purdue University. Support was also provided by NASA Space Technology Research Fellowship No. 80NSSC17K0190. This research used resources of the Advanced Photon Source, a U.S. Department of Energy (DOE) Office of Science User Facility operated for the DOE Office of Science by Argonne National Laboratory under Contract No. DE-AC02-06CH11357. Sandia National Laboratories is a multimission laboratory managed and operated by National Technology & Engineering Solutions of Sandia, LLC, a wholly owned subsidiary of NTESS, for the U.S. Department of Energy's National Nuclear Security Administration under contract DE-NA0003525. SAND #2019-????

References

[1] A.D. Casey, Z.A. Roberts, A. Satija, R.P. Lucht, T.R. Meyer, S.F. Son, Dynamic Imaging of the Temperature Field within an Energetic Composite using Phosphor Thermography, Appl. Opt. 58 (2019) 4320–4325.

[2] J. Brübach, C. Pflitsch, A. Dreizler, B. Atakan, On Surface Temperature Measurements with Thermographic Phosphors: A Review, Prog. Energy Combust. Sci. 39 (2013) 37–60.

[3] M. Aldén, A. Omrane, M. Richter, G. Särner, Thermographic Phosphors for Thermometry: A Survey of Combustion Applications, Prog. Energy Combust. Sci. 37 (2011) 422–461.

[4] G. Särner, M. Richter, M. Aldén, Investigations of Blue Emitting Phosphors for Thermometry, Meas. Sci. Technol. 19 (2008).

[5] A.H. Khalid, K. Kontis, Thermographic Phosphors for High Temperature Measurements: Principles,

Current State of the Art and Recent Applications, Sensors. 8 (2008) 5673–5744.

[6] N. Fuhrmann, J. Brübach, A. Dreizler, Phosphor Thermometry: A Comparison of the Luminescence Lifetime and the Intensity Ratio Approach, Proc. Combust. Inst. 34 (2013) 3611–3618.

[7] T. Husberg, S. Gjirja, I. Denbratt, A. Omrane, M. Aldén, J. Engström, Piston Temperature Measurement by Use of Thermographic Phosphors and Thermocouples in a Heavy-Duty Diesel Engine Run Under Partly Premixed Conditions, in: SAE International, 2005.

[8] J.T. Kashdan, B. Thirouard, S. Sae, I. Journal, J.T. Kashdan, B. Thirouard, A Comparison of Combustion and Emissions Behaviour in Optical and Metal Single-Cylinder Diesel Engines, SAE Int. J. Engines. 2 (2009) 1857–1872.

[9] T. Aizawa, H. Kosaka, Laser-induced Phosphorescence Thermography of Combustion Chamber Wall of Diesel Engine, SAE Int. J. Fuels Lubr. 1 (2009) 549–558.

[10] K.W. Tobin, S.W. Allison, M.R. Gates, G.J. Capps, D.L. Beshears, M. Cyr, B.W. Noel, High-temperature Phosphor Thermometry of Rotating Turbine Blades, AIAA J. 28 (1990) 1485–1490.

[11] P. Nau, Z. Yin, O. Lammel, W. Meier, Wall Temperature Measurements in Gas Turbine Combustors with Thermographic Phosphors, J. Eng. Gas Turbines Power. 141 (2019) 041021.

[12] J.P. Feist, a L. Heyes, S. Seefelt, Thermographic Phosphor Thermometry for Film Cooling Studies in Gas Turbine Combustors, Proc. Inst. Mech. Eng. Part A J. Power Energy. 217 (2003) 193–200.

[13] J.P. Feist, A.L. Heyes, S. Seefeldt, Thermographic Phosphors for Gas Turbines: Instrumentation Development and Measurement Uncertainties, 11th Int. Symp. Appl. Laser Tech. to Fluid Mech. (2002).

[14] M. Lawrence, H. Zhao, L. Ganippa, Gas Phase Thermometry of Hot Turbulent Jets Using Laser Induced Phosphorescence., Opt. Express. 21 (2013) 12260–12281.

[15] J.P.J. Van Lipzig, M. Yu, N.J. Dam, C.C.M. Luijten, L.P.H. De Goey, Gas-phase Thermometry in a High-pressure Cell using $BaMgAl_{10}O_{17}$:Eu as a Thermographic Phosphor, Appl. Phys. B Lasers Opt. 111 (2013) 469–481.

[16] A. Omrane, P. Petersson, M. Aldén, M.A. Linne, Simultaneous 2D Flow Velocity and Gas Temperature

Measurements using Thermographic Phosphors, Appl. Phys. B Lasers Opt. 92 (2008) 99–102.

[17] B. Fond, C. Abram, A.L. Heyes, A.M. Kempf, F. Beyrau, Simultaneous Temperature, Mixture Fraction and Velocity Imaging in Turbulent Flows using Thermographic Phosphor Tracer Particles, Opt. Express. 20 (2012) 22118–33.

[18] P.J. Potts, P.C. Webb, X-ray fluorescence spectrometry, J. Geochemical Explor. 44 (1992) 251–296.

[19] R. Jenkins, X-ray Fluorescence Spectrometry, 2nd ed., Wiley-Interscience, New York, NY, 1999.

[20] F. de Groot, A. Kotani, Core Level Spectroscopy of Solids, CRC Press, Boca Raton, FL, 2008.

[21] G. Vankó, T. Neisius, G. Molnár, F. Renz, S. Kárpáti, A. Shukla, F.M.F. De Groot, Probing the 3D Spin Momentum with X-ray Emission Spectroscopy: The Case of Molecular-spin Transitions, J. Phys. Chem. B. 110 (2006) 11647–11653.

[22] G. Vankó, J.-P. Rueff, A. Mattila, Z. Németh, A. Shukla, Temperature- and Pressure-induced Spin-state Transitions in $LaCoO_3$, Phys. Rev. B. 73 (2006) 24424.

[23] D.P. Kozlenko, N.O. Golosova, Z. Jirák, L.S. Dubrovinsky, B.N. Savenko, M.G. Tucker, Y. Le Godec, V.P. Glazkov, Temperature- and Pressure-driven Spin-state Transitions in $LaCoO_3$, Phys. Rev. B. 75 (2007) 64422.

[24] J.P. Rueff, A. Shukla, Inelastic X-ray Scattering by Electronic Excitations under High Pressure, Rev. Mod. Phys. 82 (2010) 847–896.

[25] H.K. Mao, X.J. Chen, Y. Ding, B. Li, L. Wang, Solids, Liquids, and Gases under High Pressure, Rev. Mod. Phys. 90 (2018) 15007.

[26] J. Brübach, A. Dreizler, J. Janicka, Gas Compositional and Pressure Effects on Thermographic Phosphor Thermometry, Meas. Sci. Technol. 18 (2007) 764–770.

[27] M.R. Cates, K.W. Tobin, D. Barton Smith, D.B. Smith, Evaluation of Thermographic Phosphor Technology for Aerodynamic Model Testing, Oak Ridge National Lab., TN (USA). Applied Technology Div., 1990.

[28] S. Allison, M. Cates, D. Beshears, A Survey of Thermally Sensitive Phosphors for Pressure Sensitive Paint Applications, Instrum. Aerosp. Ind. Proc. Int. Symp. 397 (2000) 29–37.

[29] C. Abram, B. Fond, F. Beyrau, High-precision Flow Temperature Imaging using ZnO Thermographic Phosphor Tracer Particles, Opt. Express. 23 (2015) 19453–19468.

[30] M. Nikl, Scintillation Detectors for X-rays, Meas. Sci. Technol. 17 (2006) R37–R54.

[31] C.W.E. Van Eijk, Inorganic Scintillators for Medical Imaging, Phys. Med. Biol. 12 (2002) R85–R106.

[32] P.A. Rodnyi, Physical Processes in Inorganic Scintillators, CRC press, 1997.

[33] S.L. Issler, C.C. Torardi, Solid State Chemistry and Luminescence of X-ray Phosphors, J. Alloys Compd. 229 (1995) 54–65.

Supplemental Material

File: Westphal et al - Proc Comb Inst 38 - Supplemental.pdf

Contents: